Bounds on the complex permittivity of matrix–particle composites

Romuald Sawicz and Kenneth Golden[a)]
Department of Mathematics, University of Utah, Salt Lake City, Utah 84112

(Received 7 June 1995; accepted for publication 28 August 1995)

The complex effective dielectric constant ϵ^* of matrix–particle composites is considered. Such composites consist of separated inclusions of material of type one embedded in a matrix of material of type two. The analytic continuation method is used to derive a series of bounds which incorporate a nonpercolation assumption about the inclusions. The key step in obtaining these improved bounds is to observe that the nonpercolation assumption restricts the support of the measure in the integral representation for ϵ^* (O. Bruno, Proc. R. Soc. London A **433**, 353 (1991)). The further the separation of the inclusions, the tighter the restriction on the support. The new bounds are applied to sea ice, which is assumed to consist of a pure ice matrix with random brine inclusions. Using experimental measurements of the average size and separation of the brine pockets, end points of the support of the measure can be determined, and subsequently used to find the allowed range of values of the effective dielectric constant of sea ice. The new bounds are compared with experimental data taken at 4.75 GHz, and exhibit significant improvement over previous fixed volume fraction and Hashin–Shtrikman bounds. © *1995 American Institute of Physics.*

I. INTRODUCTION

Because of the difficulty of calculating the effective parameters (e.g., dielectric constant, or thermal or electrical conductivity) of heterogeneous media, there has been much effort devoted to obtaining bounds for these parameters. The first remarkable result was obtained by Wiener.[1] He found optimal bounds for the effective parameters of a multicomponent material with fixed volume fractions and real component parameters. For the isotropic case these bounds were improved by Hashin and Shtrikman[2] using a variational formulation of the problem.

Bergman[3–5] and Milton[6,7] independently introduced a new method for obtaining bounds on complex effective parameters which does not rely on variational principles, but exploits the properties of the effective parameters as analytic functions of the component parameters. A mathematical formulation of it was given by Golden and Papanicolaou;[8] first in the case of two-component materials, where the effective parameters are functions of a single complex variable—the ratio of the two component parameters. Subsequently they extended the method to the multicomponent case.[9]

The integral representation they found involves a complex kernel containing the component parameter information and a positive measure containing information about the geometry of the composite. The moments of the measure, which introduce geometric information most conveniently, are related to a perturbation expansion of the material about a homogeneous medium. The bounds were obtained by evaluating the formula over the set of the extremal points of the set of admissible measures. They can be improved if additional information about the microstructure is known.

In this article we investigate the effective dielectric constant ϵ^* of matrix–particle composites, which consist of separated inclusions of phase one embedded in a matrix of the other material. This kind of microstructure is prevalent in nature. An example of such a composite is sea ice, or frozen sea water, which consists of a pure ice matrix with random brine and air inclusions. The effect of air inclusions on ϵ^* is often ignored, particularly for young sea ice, which typically has very low air content. Here we will assume the sea ice to be a two-phase composite.

In Ref. 10, Golden compares the experimental data on ϵ^* at 4.75 GHz obtained in Ref. 11 with the fixed volume fraction and Hashin–Shtrikman bounds on the complex effective dielectric constant of sea ice. One can notice that the data consistently lie in the lower left-hand corner of the bounds, i.e., where $\mathrm{Re}(\epsilon^*)$ and $\mathrm{Im}(\epsilon^*)$ are minimal. This observation suggests that the ice phase is dominating the behavior, which reflects the microstructural feature that the brine is contained in inclusions, and does not form a connected matrix.

In this article we derive improved complex bounds on the effective dielectric constant of matrix–particle composites using the analytic continuation method. Our results rely on the work of Bruno,[12] who has found restrictions on the support of the measure in the integral representation for ϵ^*, which arise from imposing the geometrical condition that one phase be contained in separated inclusions embedded in a matrix of the other material. These restrictions are used to derive a new integral representation. We obtain the complex bounds by applying a series of extremal procedures[8] to this integral representation. The improved bounds capture more tightly the data for ϵ^* of sea ice in Ref. 11 than the previous bounds found in Ref. 10.

II. BOUNDS ON THE COMPLEX PERMITTIVITY OF COMPOSITE MATERIALS BY ANALYTIC CONTINUATION

In order to describe the series of bounds we have been developing, let us briefly review the analytic continuation method for studying the effective properties of composite materials. For simplicity we consider a random medium in all of R^d. Let $\epsilon(x,\omega)$ be a (spatially) stationary random field in $x \in R^d$ and $\omega \in \Omega$, where Ω is the set of all realizations of

a)Electronic mail: Golden@math.utah.edu

 0021-8979/95/78(12)/7240/7/$6.00

our random medium. We assume $\epsilon(x,\omega)$ takes the values ϵ_1 and ϵ_2, which are complex numbers, and write

$$\epsilon(x,\omega)=\epsilon_1\chi_1(x,\omega)+\epsilon_2\chi_2(x,\omega), \tag{2.1}$$

where χ_j is the characteristic function of the medium $j=1,2$, which equals one for all realizations $\omega\in\Omega$ having medium j at x, and otherwise equals zero. Let $E(x,\omega)$ and $D(x,\omega)$ be the stationary random electric and displacement fields satisfying

$$D(x,\omega)=\epsilon(x,\omega)E(x,\omega), \tag{2.2}$$

$$\nabla\cdot D(x,\omega)=0, \tag{2.3}$$

$$\nabla\times E(x,\omega)=0, \tag{2.4}$$

$$\langle E(x,\omega)\rangle=e_k, \tag{2.5}$$

where e_k is a unit vector in the kth direction, for some $k=1,\ldots,d$, and $\langle\cdot\rangle$ means the ensemble average over Ω or the spatial average over all of R^d.

In view of the local constitutive law (2.2), the effective complex permittivity tensor $\boldsymbol{\epsilon}^*$ is defined as

$$\langle D\rangle=\boldsymbol{\epsilon}^*\langle E\rangle. \tag{2.6}$$

For simplicity, we focus on one diagonal coefficient $\epsilon^* = \epsilon^*_{kk}$. Due to the homogeneity of effective parameters, $\epsilon^*(\lambda\epsilon_1,\lambda\epsilon_2)=\lambda\epsilon^*(\epsilon_1,\epsilon_2)$, ϵ^* depends only on the ratio $h=\epsilon_1/\epsilon_2$, and we define $m(h)=\epsilon^*/\epsilon_2$. The two main properties of $m(h)$ are that it is analytic off $[-\infty,0]$ in the h plane, and that it maps the upper half-plane to the upper half-plane,[4,8] so that it is an example of a Herglotz function.

The key step in the analytic continuation method is obtaining an integral representation for ϵ^*. For this purpose it is more convenient to look at the function[4]

$$F(s)=1-m(h)=1-\frac{\epsilon^*}{\epsilon_2},\quad s=1/(1-h),\quad h=\frac{\epsilon_1}{\epsilon_2}, \tag{2.7}$$

which is analytic off $[0,1]$ in the s plane. It was then proven in Ref. 8 that $F(s)$ has the following representation:

$$F(s)=\int_0^1\frac{d\mu(z)}{s-z},\quad s\notin[0,1], \tag{2.8}$$

where μ is a positive measure on $[0,1]$. One of the most important features of Eq. (2.8) is that it separates the parameter information in $s=1/(1-\epsilon_1/\epsilon_2)$ from information about the geometry of the mixture, which is all contained in μ. Actually, μ is the spectral measure associated with the operator $\Gamma\chi_1$, where $\Gamma=\nabla(\Delta)^{-1}\nabla\cdot$, and χ_1 is the characteristic function of medium 1, equaling 1 in medium 1 (and 0 otherwise), which determines the geometry.

Statistical assumptions about the geometry are incorporated into μ through its moments

$$\mu_n=\int_0^1 z^n d\mu(z). \tag{2.9}$$

Comparison of a perturbation expansion of Eq. (2.8) around a homogeneous medium ($s=\infty$, or $\epsilon_1=\epsilon_2$) with a similar expansion of a resolvent representation for $F(s)$,[8] yields

$$\mu_n=(-1)^n\langle\chi_1[(\Gamma\chi_1)^n\cdot e_k]e_k\rangle. \tag{2.10}$$

Then

$$\mu_0=p_1, \tag{2.11}$$

if only the volume fractions are known, and

$$\mu_1=\frac{p_1p_2}{d}, \tag{2.12}$$

if the material is statistically isotropic, where d is the dimension of the system. In general, knowledge of the $(n+1)$-point correlation function of the medium allows calculation of μ_n (in principle).

Bounds on ϵ^*, or $F(s)$, are obtained by fixing s in Eq. (2.8), varying over admissible measures μ (or admissible geometries), such as those that satisfy only Eq. (2.11), and finding the corresponding range of values of $F(s)$ in the complex plane. Two types of bounds on ϵ^* are obtained. The first bound R_1 assumes only that the relative volume fractions p_1 and $p_2=1-p_1$ of the ice and brine are known, so that Eq. (2.11) is satisfied. In the F plane, the region R_1 is bounded by circular arcs, one of which is parametrized by

$$C_1(z)=\frac{p_1}{s-z},\quad 0\leqslant z\leqslant p_2. \tag{2.13}$$

To exhibit the other arc, it is convenient to consider the auxiliary function

$$E(s)=1-\frac{\epsilon_1}{\epsilon^*}=\frac{1-sF(s)}{s[1-F(s)]}, \tag{2.14}$$

which is a Herglotz function like $F(s)$, analytic off $[0,1]$. Then in the E plane, we can parametrize the other circular boundary of R_1 by

$$\hat{C}_1(z)=\frac{p_2}{s-z},\quad 0\leqslant z\leqslant p_1. \tag{2.15}$$

In the ϵ^* plane, R_1 has vertices $p_1\epsilon_1+p_2\epsilon_2$ and $(p_1/\epsilon_1+p_2/\epsilon_2)^{-1}$, and collapses to the interval

$$(p_1/\epsilon_1+p_2/\epsilon_2)^{-1}\leqslant\epsilon^*\leqslant p_1\epsilon_1+p_2\epsilon_2 \tag{2.16}$$

when ϵ_1 and ϵ_2 are real, which are the classical arithmetic and harmonic mean bounds. The complex bounds (2.13) and (2.15) are optimal and can be attained by a composite of uniformly aligned spheroids of material one in all sizes coated with confocal shells of material two, and vice versa. These arcs are traced out as the aspect ratio varies.

If the material is further assumed to be statistically isotropic, i.e., $\epsilon_{ik}=\epsilon^*\delta_{ik}$, then Eq. (2.12) must be satisfied as well. A convenient way of including this information is to use the transformation of Ref. 3,

$$F_1(s)=\frac{1}{p_1}-\frac{1}{sF(s)}. \tag{2.17}$$

The function $F_1(s)$ is, again, a Herglotz function which has the representation

$$F_1(s)=\int_0^1\frac{d\mu^1(z)}{s-z}. \tag{2.18}$$

The constraint (2.12) on $F(s)$ is then transformed to a restriction of only the mass, or zeroth moment μ_0^1 of μ^1, with

$$\mu_0^1 = p_2/p_1 d. \tag{2.19}$$

Applying the same procedure as for R_1 yields the bound R_2, where the boundaries are again circular arcs. In the F plane, one of these arcs is parametrized by

$$C_2(z) = \frac{p_1(s-z)}{s(s-z-p_1/d)}, \quad 0 \leq z \leq (d-1)/d. \tag{2.20}$$

In the E plane, the other arc is parametrized by

$$\hat{C}_2(z) = \frac{p_2(s-z)}{s[s-z-p_1(d-1)/d]}, \quad 0 \leq z \leq 1/d. \tag{2.21}$$

When ϵ_1 and ϵ_2 are real with $\epsilon_1 \leq \epsilon_2$, R_2 collapses to the interval

$$\epsilon_1 + p_2 \Big/ \left(\frac{1}{\epsilon_2 - \epsilon_1} + \frac{p_1}{d\epsilon_1} \right) \leq \epsilon^* \leq \epsilon_2 + p_1 \Big/ \left(\frac{1}{\epsilon_1 - \epsilon_2} + \frac{p_2}{d\epsilon_2} \right), \tag{2.22}$$

which are the Hashin–Shtrikman bounds.[2] We remark that higher-order correlation information can be conveniently incorporated by iterating Eq. (2.17), as in Ref. 13.

To summarize, R_1 is a region in the complex ϵ^* plane, bounded by circular arcs, in which ϵ^* for any microgeometry with the given volume fractions must lie. In addition to the volume fractions, the second bound R_2 assumes that the material is statistically isotropic within the horizontal plane, so that we take $d=2$. The region R_2 is again bounded by circular arcs, and lies inside R_1. These bounds are compared in Ref. 10 with the experimental data found by Arcone, Gow, and McGrew[11] for artificially grown sea ice at 4.75 and 9.5 GHz.

III. IMPROVED BOUNDS ON THE COMPLEX PERMITTIVITY OF SEA ICE AS A MATRIX–PARTICLE COMPOSITE

In Ref. 10, a striking feature of the figures illustrating the comparison of the experimental data for sea ice with the bounds R_1 and R_2 is that the data consistently lie in the lower left-hand corner of the bounds, i.e., where $\mathrm{Re}(\epsilon^*)$ and $\mathrm{Im}(\epsilon^*)$ are minimal. This observation suggests that the ice phase is dominating the behavior, which reflects the microstructural feature that the brine is contained in inclusions, and does not form a connected matrix.

In order to try and capture the data in Ref. 11 more closely, we incorporate the nonpercolation assumption about the inclusions into our series of bounds, by turning to the work of Bruno.[12] In this seminal paper, Bruno has found restrictions on the support of μ in the integral representation (2.8) which arise from imposing the geometrical condition that one phase be contained in separated inclusions embedded in a matrix of the other material. The further the separation, the tighter the restriction on the support. Based on this support restriction, Bruno has derived bounds on the effective conductivity, in the case of real component conductivities, of some matrix–particle composites.

One of the reasons for developing bounds based on the matrix–particle assumption is that more general bounds begin to break down, and become trivial in the high contrast limit. For example, as $\epsilon_2 \to \infty$ in Eq. (2.22), the upper Hashin–Shtrikman bound diverges. For composites made of highly contrasting components, such as the ice and brine of sea ice, such bounds which do not become trivial are clearly of significant use.

To describe the new complex bounds, we must first briefly review[12,14] the main ideas of Bruno's work on how the matrix–particle assumption restricts the support of the measure μ. While the general, stationary random formulation of the effective permittivity problem given in Sec. II is still valid, it is perhaps more useful at this point, given that we are considering a specific class of possible geometries, to focus on this spatial dependence.

Let us consider a material occupying a cubic (or square) box Λ in R^d, with $0 \leq x_i \leq 1$, $1 \leq i \leq d$. We assume that the material consists of a matrix of permittivity ϵ_1 containing a finite, arbitrarily large number of nontouching grains of permittivity ϵ_2. The region of Λ occupied by ϵ_1 will be referred to as the outside region, denoted by Λ^{out}, and the inside region containing ϵ_2 is denoted by Λ^{in}. We assume that Λ is very large compared to the microstructural scale, which is determined by the size and spacing of the inclusions. The local permittivity $\epsilon(x)$ is still given by Eq. (2.1). For simplicity, the inclusions are assumed to be connected regions with smooth boundaries. If the upper and lower faces of Λ are kept at constant potentials $\Phi(x_d=1)=1$ and $\Phi(x_d=0)=0$, the electric potential Φ inside the box Λ satisfies

$$\nabla \cdot (\epsilon \nabla \Phi) = 0, \tag{3.1}$$

with the boundary condition $\partial\Phi/\partial n = 0$ along the vertical walls, as well as the equipotential condition on the top and bottom faces. The effective permittivity is then defined by

$$\epsilon^* = \int_\Lambda \epsilon \frac{\partial \Phi}{\partial x_d} \, dV, \tag{3.2}$$

or equivalently by

$$\epsilon^* = \int_\Lambda \epsilon |\nabla \Phi|^2 dV. \tag{3.3}$$

Correspondence with Sec. II is obtained by taking the limit as the microstructural scale$\to$0, or as the volume becomes infinite, with appropriate normalization in Eqs. (3.2) and (3.3). See Ref. 8, for example. Again it will be important to consider the functions

$$m(h) = \frac{\epsilon^*}{\epsilon_2}, \quad h = \frac{\epsilon_1}{\epsilon_2} \tag{3.4}$$

and

$$F(s) = 1 - m(h), \quad s = \frac{1}{1-h}. \tag{3.5}$$

Recall that general arguments alone yield only that $m(h)$ is analytic off $(-\infty,0]$ in the h plane, while $F(s)$ is analytic off $[0,1]$ in the s plane. Note that Φ is harmonic in Λ^{out} and Λ^{in}, i.e.,

$$\Delta\Phi^{\text{in}}=\Delta\Phi^{\text{out}}=0. \tag{3.6}$$

Across the boundary γ separating Λ^{out} and Λ^{in}, Φ must be continuous, and yield continuity of the normal component of $D=\epsilon E$.

Now, the physical observation which underlies the restriction of the spectral measure is that in high contrast media with inclusions, energy is concentrated where the inclusions begin to touch. If these situations can be avoided, then the energy can be controlled. In particular, if we consider a class of media $C_{A,B}$,[12] *defined* in terms of control on the energy, then one can obtain the estimates necessary to get convergence of a series which allows further analytic continuation of $m(h)$ or $F(s)$ beyond the domains given in Sec. II. For definition of the class and more details, see Ref. 12. In the same paper the following theorem is proved for materials in the class $C_{A,B}$.

Theorem 3.1. The (normalized) effective permittivity $m(h)$ is analytic off the interval $[-B,-1/A]$ in the h plane.

We remark that the main idea used in establishing the above theorem is to obtain convergence of the expansion

$$\Phi(x,h)=\sum_{i=0}^{\infty}\Phi_i(x)h^i. \tag{3.7}$$

As a consequence of Theorem 3.1, the support of the measure μ in the integral representation (2.8) for $F(s)$ is contained in the interval

$$s_m\leqslant s\leqslant s_M \tag{3.8}$$

$[s_m,s_M]\subset[0,1]$, where

$$s_m=\frac{1}{1+B},\quad s_M=\frac{A}{A+1}. \tag{3.9}$$

Then Eq. (2.8) takes the form

$$F(s)=\int_{s_m}^{s_M}\frac{d\mu(z)}{s-z}. \tag{3.10}$$

To obtain complex bounds on ϵ^* which incorporate the matrix–particle assumption for type $C_{A,B}$ materials, we exploit the restricted representation (3.10), for given values of s_m and s_M. We will describe later how these values are chosen for relevant sea ice microgeometries.

In the standard sequence of bounds on ϵ^* (e.g., Ref. 13), the first one normally considered is the so-called "zeroth-order" bound, where one assumes only that the permittivities of the constituents are known, and nothing about the geometry is assumed. In terms of Eq. (2.8), the only assumption imposed on F is $F(s=1)\leqslant 1$, and that the mass μ_0 of μ satisfies $\mu_0\leqslant 1$. A convenient way of incorporating the support restriction is to first consider a new variable t, defined by

$$s=(s_M-s_m)t+s_m. \tag{3.11}$$

Then the interval $[s_m,s_M]$ in the s plane gets mapped to $[0,1]$ in the t plane, and the function

$$H(t)=F(s)=F[(s_M-s_m)t+s_m] \tag{3.12}$$

is analytic off $[0,1]$ in the complex t plane. It can be shown that there is a positive Borel measure ν on $[0,1]$ such that

$$H(t)=\int_0^1\frac{d\nu(z)}{t-z}. \tag{3.13}$$

Letting

$$\lambda=s_M-s_m \tag{3.14}$$

be the spectral width, it can be shown using Eqs. (2.11) and (2.12) that

$$\nu_0=\frac{p_1}{\lambda}\leqslant 1, \tag{3.15}$$

if only the volume fractions are known, and

$$\nu_1=\frac{p_1}{\lambda^2}\left(\frac{p_2}{d}-s_m\right), \tag{3.16}$$

if the material is statistically isotropic.

Now, if we view Eq. (3.13) for fixed t as a linear functional in ν, then the allowed region in the H plane is the image of admissible measures, which forms a compact, convex set whose extreme points are of the form

$$\nu=\alpha\delta_z, \tag{3.17}$$

which are Dirac point measures of mass α concentrated at z. For such measures H has the form

$$H(t)=\frac{\alpha}{t-z}. \tag{3.18}$$

Then the allowed region in the complex H plane is the image under Eq. (3.18) of the triangle in (α,z) space,

$$\alpha+z\leqslant 1,\quad 0\leqslant\alpha\leqslant 1,\quad 0\leqslant z<1. \tag{3.19}$$

This region is bounded by a circular arc parametrized by

$$\frac{\alpha}{t-1+\alpha},\quad 0\leqslant\alpha\leqslant 1, \tag{3.20}$$

and a line segment parametrized by

$$\frac{\alpha}{t},\quad 0\leqslant\alpha\leqslant 1. \tag{3.21}$$

In view of Eq. (3.12) the allowed region Q_0 in the ϵ^* plane is bounded by a circular arc $C(\alpha)$

$$C(\alpha)=\epsilon_2\frac{\epsilon_2-s_M(\epsilon_2-\epsilon_1)}{\epsilon_2+(\epsilon_2-\epsilon_1)[s_M+\alpha(s_M-s_m)]},\quad 0\leqslant\alpha\leqslant 1, \tag{3.22}$$

and a line segment

$$L(\alpha)=\epsilon_2\frac{-\epsilon_2+(\epsilon_2-\epsilon_1)[\alpha(s_M-s_m)+s_m]}{-\epsilon_2+s_m(\epsilon_2-\epsilon_1)},\quad 0\leqslant\alpha\leqslant 1. \tag{3.23}$$

The vertices of the region are $w_1=\epsilon_1$, and

$$w_2=\frac{\epsilon_1(-\epsilon_1+s_M\epsilon_1-s_M\epsilon_2)}{-\epsilon_1+s_m\epsilon_1-s_m\epsilon_2}. \tag{3.24}$$

For real parameters $\epsilon_1\leqslant\epsilon_2$, Q_0 collapses to the interval

$$\epsilon_1\leqslant\epsilon^*\leqslant\frac{\epsilon_1(-\epsilon_1+s_M\epsilon_1-s_M\epsilon_2)}{-\epsilon_1+s_m\epsilon_1-s_m\epsilon_2}. \tag{3.25}$$

As indicated in Eq. (2.11), if one assumes that the relative volume fractions of the two constituents are known, then the mass μ_0 of μ satisfies $\mu_0=p_1$. In order to get complex bounds on ϵ^* for $C_{A,B}$ materials, it is useful at this point to briefly review how the arcs $C_1(z)$ and $\hat{C}_1(z)$ in Eqs. (2.13) and (2.15), respectively, are obtained.[13] For $F(s)$ having the representation (2.8), with $\mu_0=p_1$, the possible range of values of $F(s)$ lie inside the circle

$$C_1(z)=\frac{p_1}{s-z},\quad -\infty\leqslant z\leqslant\infty, \tag{3.26}$$

in the F plane. Furthermore, the possible range of values of $E(s)=1-\epsilon_1/\epsilon^*$ lie inside the circle

$$\hat{C}_1(z)=\frac{p_2}{s-z},\quad -\infty\leqslant z\leqslant\infty, \tag{3.27}$$

in the the E plane. Intersection of these two circles leads to the region R_1 given in Sec. II. Incorporation of knowledge of μ_1 is accomplished with transformations of the type in Eq. (2.17), applied to F and E.

Now we apply this procedure to $H(t)$, so that in the H plane its possible range of values lies in the circle

$$K_1'(z)=\frac{p_1/\lambda}{t-z},\quad -\infty\leqslant z\leqslant\infty. \tag{3.28}$$

In the F plane this translates into the circle

$$K_1(z)=\frac{p_1}{s-s_m-z(s_M-s_m)},\quad -\infty\leqslant z\leqslant\infty, \tag{3.29}$$

which happens to coincide with the circle $C_1(z)$ in Eq. (3.26). Now we consider the analog of $E(s)$ which is the companion of $H(t)$. Let

$$G(t)=E(s)=E[(s_M-s_m)t+s_m], \tag{3.30}$$

with

$$G(t)=\frac{1-tH(t)}{t[1-H(t)]}. \tag{3.31}$$

Then $G(t)$ has an integral representation

$$G(t)=\int_0^1\frac{d\rho(z)}{t-z}, \tag{3.32}$$

where the mass of ρ is

$$\rho_0=1-\frac{p_1}{\lambda}. \tag{3.33}$$

We then obtain a circle in the G plane analogous to Eq. (3.28), which in the E plane becomes

$$\hat{K}_1(z)=\frac{s_M-s_m-p_1}{s-s_m-zs_M+zs_m},\quad -\infty\leqslant z\leqslant\infty. \tag{3.34}$$

Back in the ϵ^* plane, the intersection of these two circles yields a region Q_1 which has vertices

$$v_1=\epsilon_2\frac{-\epsilon_2+(\epsilon_2-\epsilon_1)(s_m+p_1)}{-\epsilon_2+s_m(\epsilon_2-\epsilon_1)}, \tag{3.35}$$

$$v_2=\epsilon_2\frac{-\epsilon_2+s_M(\epsilon_2-\epsilon_1)}{-\epsilon_2+(\epsilon_2-\epsilon_1)(s_M-p_1)}. \tag{3.36}$$

For $s_m=0$ and $s_M=1$ they coincide with the arithmetic and harmonic mean formulas, as expected. If ϵ_1 and ϵ_2 are real and positive, Q_1 reduces to the interval

$$\epsilon_2\frac{\epsilon_2(1-s_M)+\epsilon_1 s_M}{\epsilon_2(1-s_M+p_1)+\epsilon_1(s_M-p_1)}\leqslant\epsilon^*\leqslant\epsilon_2\frac{\epsilon_2(1-s_m-p_1)+\epsilon_1(s_m+p_1)}{\epsilon_2(1-s_m)+\epsilon_1 s_m}. \tag{3.37}$$

Finally, we consider the case where the material is further assumed to be statistically isotropic. Let

$$H_1(t)=\frac{1}{\nu_0}-\frac{1}{tH(t)}=\frac{s_M-s_m}{p_1}-\frac{1}{tH(t)}. \tag{3.38}$$

Then H_1 is a Herglotz function which is analytic off [0,1] and has an integral representation in terms of a measure ν^1, which can be shown to have mass

$$\nu_0^1=\frac{\nu_1}{(\nu_0)^2}=\frac{p_2/d-s_m}{p_1}. \tag{3.39}$$

Then the allowed values of $H_1(t)$ are contained inside the circle $\nu_0^1/(t-z)$, $-\infty\leqslant z\leqslant\infty$, which becomes in the F plane the circle

$$K_2(z)=\frac{p_1[s-s_m-z(s_M-s_m)]}{(s-s_m)[s-p_2/d-z(s_M-s_m)]},\quad -\infty\leqslant z\leqslant\infty. \tag{3.40}$$

For $s_m=0$ and $s_M=1$ the above circle is identical to the full circle containing the arc (2.20).

To obtain the other circle, we apply a similar transformation to $G(t)$, obtaining a function

$$G_1(t)=\frac{1}{\rho_0}-\frac{1}{tH(t)}=\frac{s_M-s_m}{s_M-s_m-p_1}-\frac{1}{tH(t)}, \tag{3.41}$$

which, again, is a Herglotz function analytic off [0,1] with the representing measure ρ^1 of mass

$$\rho_0^1=\frac{\rho_0(1-\rho_0)-\rho_1}{(1-\rho_0)^2}=\frac{p_1(ds_M-p_1-1)}{d(s_M-s_m-p_1)^2}. \tag{3.42}$$

Then in the G^1 plane, the allowed values are contained inside the circle

$$K_2'(z)=\frac{p_1(ds_M-p_1-1)}{d(s_M-s_m-p_1)^2(t-z)},\quad -\infty\leqslant z\leqslant\infty. \tag{3.43}$$

The intersection of the two circular regions (in a common plane) yields a region Q_2 bounded by circular arcs, with vertices in the ϵ^* plane at

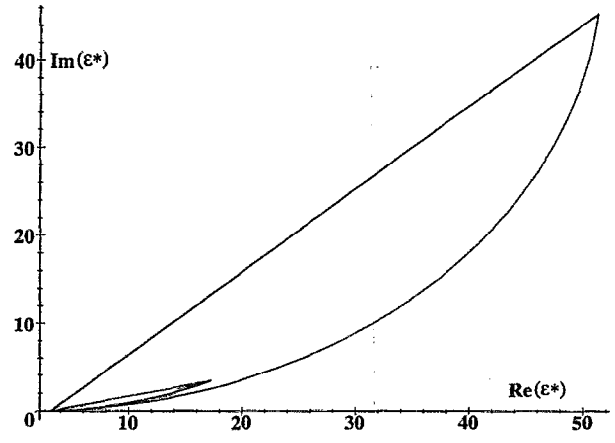

FIG. 1. Zeroth-order bounds R_0 (outer) and the improved zeroth-order bounds Q_0 (inner) for sea ice with the frequency $f=4.75$ GHz, salinity $S=0.41\%$, temperature $T=-6$ °C, $\epsilon_1=3.15+i0.002$, $\epsilon_2=51+i45$. To find Q_0, the brine inclusions are assumed to have security spheres for which the minimal ratio of the radius of the inclusion to the radius of the security sphere q is not greater than 0.8. This corresponds to the end points of the support of the measure μ at the points $s_m=0.18$ and $s_M=0.82$.

$$v_1'=\epsilon_1\frac{s_M\eta+\epsilon_1}{s_m\eta+\epsilon_1}\left(1+\left(\frac{\lambda-p_2}{\delta}\right)^2\Bigg/\left(\frac{(p_2-\lambda)(s_M\eta+\epsilon_1)}{\lambda^2\eta}\right)+\frac{p_2(p_1-ds_m)}{d\lambda^2}\right), \tag{3.44}$$

$$v_2'=\epsilon_1+p_2\Bigg/\left(\frac{1}{\eta}+\frac{p_1}{d\epsilon_1}\right), \tag{3.45}$$

where

$$\eta=\epsilon_2-\epsilon_1, \quad \lambda=s_M-s_m. \tag{3.46}$$

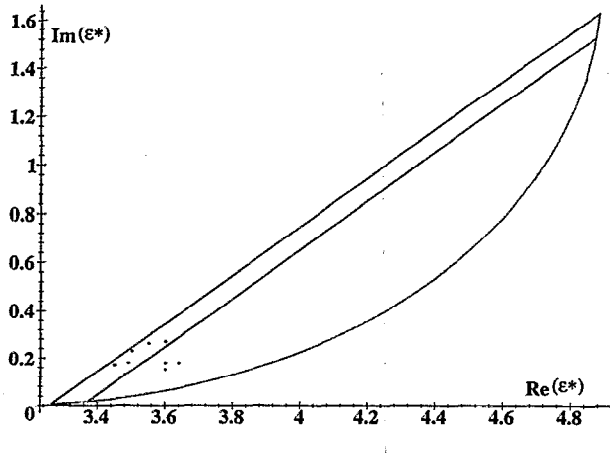

FIG. 2. Comparison of experimental data with the volume fraction bounds R_1 (outer) and the improved volume fraction bounds Q_1 (inner) for sea ice with the frequency $f=4.75$ GHz, salinity $S=0.41\%$, temperature $T=-6$ °C, $\epsilon_1=3.15+i0.002$, $\epsilon_2=51+i45$, and the brine volume fraction $p_2=0.036$. To find Q_1, the brine inclusions are assumed to have security spheres for which the minimal ratio of the radius of the inclusion to the radius of the security sphere q is not greater than 0.8. This corresponds to the end points of the support of the measure μ at the points $s_m=0.18$ and $s_M=0.82$.

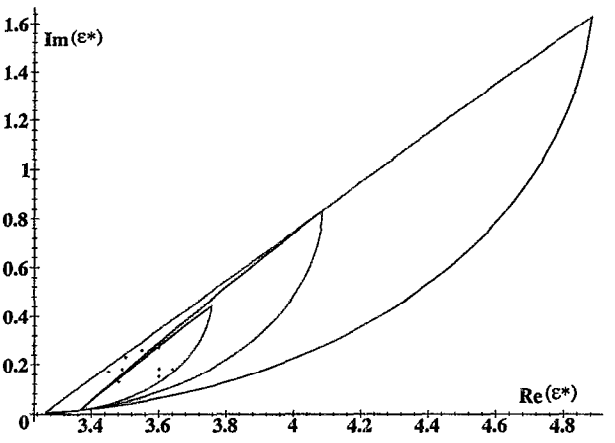

FIG. 3. Experimental data, volume fraction (outer), Hashin–Shtrikman, and improved Hashin–Shtrikman (inner) bounds on the complex effective dielectric constant of sea ice with the frequency $f=4.75$ GHz, salinity $S=0.41\%$, temperature $T=-6$ °C, $\epsilon_1=3.15+i0.002$, $\epsilon_2=51+i45$, and the volume of brine $p_2=0.036$. To find improved Hashin–Shtrikman bounds, the brine inclusions are assumed to have security spheres for which the minimal ratio of the radius of the inclusion to the radius of the security sphere q is not greater than 0.8. This corresponds to the end points of the support of the measure μ at the points $s_m=0.18$ and $s_M=0.82$.

Note that the vertex v_2' is the lower Hashin–Shtrikman expression, so that it coincides with the same vertex from the region R_2. When the local dielectric constants ϵ_1 and ϵ_2 are positive with $\epsilon_1\leqslant\epsilon_2$, it collapses to the interval

$$\epsilon_1+p_2\Bigg/\left(\frac{1}{\eta}+\frac{p_1}{2\epsilon_1}\right)\leqslant\epsilon^*\leqslant\epsilon_1\frac{s_M\eta+\epsilon_1}{s_m\eta+\epsilon_1}\left(1+\left(\frac{\lambda-p_2}{\lambda}\right)^2\Bigg/\left(\frac{(p_2-\lambda)(s_M\eta+\epsilon_1)}{\lambda^2\eta}\right)+\frac{p_2(p_1-ds_m)}{d\lambda^2}\right). \tag{3.47}$$

Now let us describe how the new complex bounds are compared with the data on complex ϵ^* from Ref. 11. For a sample of sea ice at a given temperature and salinity, we compute the ϵ_2 and p_2 for brine the same as in Ref. 10. Now we assume that we are looking at a horizontal slice of sea ice with $d=2$, so that it is reasonable to assume that the brine phase is contained in separated inclusions. We will further assume that the brine is contained in circular disks, which allows us to utilize the explicit calculations in Ref. 12 of the constants A and B, as well as s_m and s_M. Our class of materials then is as follows. Disks of brine of radius r_b hold random positions in a host of ice, in such a way that each disk of brine is surrounded by a "corona" of ice, with outer radius r_i. Then the minimal separation of brine inclusions is $2(r_i-r_b)$. Such a medium is called a q material, where $q=r_b/r_i$. Using typical brine inclusion sizes from Ref. 15, we assume $r_b=0.2$ mm. Now, the longest typical separation distance between brine pockets is across a basal plane of the platelets present in formation, and this distance averages 0.6 mm. However, along a basal plane these separations are usu-

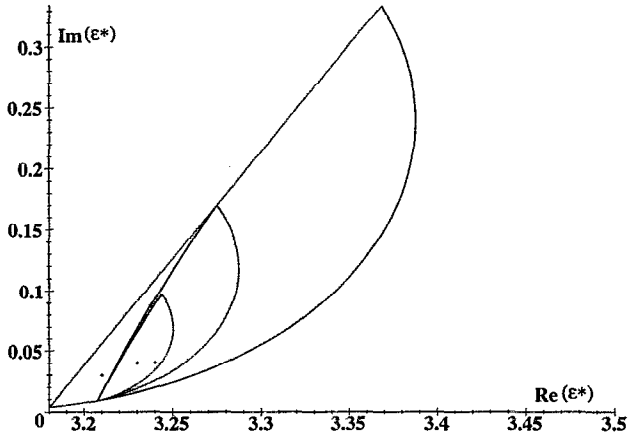

FIG. 4. Experimental data, volume fraction (outer), Hashin–Shtrikman, and improved Hashin–Shtrikman (inner) bounds on the complex effective dielectric constant of sea ice with the frequency $f=4.75$ GHz, salinity $S=0.41\%$, temperature $T=-11$ °C, $\epsilon_1=3.15+i0.002$, $\epsilon_2=42.2+i45.6$, and the volume of brine $p_2=0.0205$. To find improved Hashin–Shtrikman bounds, the brine inclusions are assumed to have security spheres for which the minimal ratio of the radius of the inclusion to the radius of the security sphere q is not greater than 0.8. This corresponds to the end points of the support of the measure μ at the points $s_m=0.18$ and $s_M=0.82$.

ally smaller. As a lower bound on these separations, we take 0.1 mm. Then $r_i=0.25$ and $q=0.8$. From Ref. 12, we have for $d=2$

$$s_m=\tfrac{1}{2}(1-q^2), \quad s_M=\tfrac{1}{2}(1+q^2), \tag{3.48}$$

so that $s_m=0.18$ and $s_M=0.82$. Figure 1 shows a comparison of the region Q_0 with the zeroth-order bounds R_0 in Ref. 10. The region R_0 is bounded by Eqs. (3.22) and (3.23) where $s_m=0$ and $s_M=1$. In Fig. 2, the region Q_1 is compared with R_1 and experimental data. Q_1 is the lens-shape region inside R_1, bounded from below by the curve which coincides with the arc circle $C_1(z)$ in Eq. (3.26). Finally, in Figs. 3 and 4 we compare experimental data in Ref. 11 for two different temperatures (and brine volumes) with the regions R_1, R_2, and Q_2. The region Q_2 is the innermost one, inside R_1 and R_2. The agreement is very good. Discrepancies are accounted for here by small uncertainties in the brine volume of the actual data, and a slight degree of anisotropy, which was observed in some of the samples. Nevertheless, Q_2 is a significant improvement for matrix–particle composites over the more general bounds R_1 and R_2.

ACKNOWLEDGMENTS

The authors are pleased to thank G. Milton and O. Bruno for helpful conversations. We gratefully acknowledge the support of ONR Grant No. N000149310141 and NSF Grant No. DMS-9307324, as well as an AASERT Graduate Student Supplement to the ONR Grant.

[1] O. Wiener, Abhandl. Math-Phys. Kl. Königl.Sachsischen Ges. **32**, 509 (1912).
[2] Z. Hashin and S. Shtrikman, J. Appl. Phys. **33**, 3125 (1962).
[3] D. J. Bergman, Ann. Phys. **138**, 78 (1982).
[4] D. J. Bergman, Phys. Rep. C **43**, 377 (1978).
[5] D. J. Bergman, Phys. Rev. Lett. **44**, 1285 (1980).
[6] G. W. Milton, Appl. Phys. Lett. **37**, 300 (1980).
[7] G. W. Milton, Phys. Rev. Lett. **46**, 542 (1981).
[8] K. Golden and G. Papanicolaou, Commun. Math. Phys. **90**, 473 (1983).
[9] K. Golden and G. Papanicolaou, J. Stat. Phys. **40**, 655 (1985).
[10] K. Golden, J. Geophys. Res. (in press).
[11] S. A. Arcone, A. J. Gow, and S. McGrew, J. Geophys. Res. **91**, 14281 (1986).
[12] O. Bruno, Proc. R. Soc. London Ser. A **433**, 353 (1991).
[13] K. Golden, J. Mech. Phys. Solids **34**, 333 (1986).
[14] O. Bruno, in *Calculus of Variations, Homogenization and Continuum Mechanics*, edited by G. Bouchitté, G. Butazzo, and P. Suquet (World Scientific, Singapore, 1994), pp. 99–115.
[15] W. F. Weeks and S. F. Ackley, CRREL Monograph **82-1** (1982).